Effect of Close-Packed Plane Boundaries in a Bain Zone on the Crack Path in Simulated Coarse-Grained HAZ of Bainitic Steel

HIDENORI TERASAKI, YUTARO SHINTOME, YU-ICHI KOMIZO, MITSURU OHATA, KOJI MORIGUCHI, and YUSAKU TOMIO

Global effect of Bain-zone boundaries and the local effect of close-packed plane (CP) boundaries on the path of secondary cleavage cracks (observed on a fractured V-notch Charpy specimen) were visualized and discussed in simulated coarse-grained HAZ of bainitic steel. Microstructural unit map (Bain-zone map and CP map) was obtained by electron backscatter diffraction method for a prior austenite grain of a few hundred micrometers. Furthermore, a correlation between CP boundaries and sites that favored formation of the blocky martensite–austenite (M–A) constituent was confirmed. It was clarified that two crack deviation/local changing factors (CP boundaries and blocky M–A) are paired.

I. INTRODUCTION

FROM the viewpoint of production efficiency, high heat input welding is demanded in welded structures constructed using high-strength steel. However, high heat input welding causes embrittlement at the coarse-grained heat-affected zones (CGHAZs), and a critical cooling rate exists during welding process. Therefore, understanding the relation between the microstructure of the CGHAZ formed during high heat input welding of high-strength steel (bainite and/or martensite) and the steel's fracture properties, such as its crack resistance, is essential.

The literature contains numerous studies of the relation between the microstructure of the CGHAZ of bainitic steel and the change in the crack path. Gourgues et al.[1] showed a correlation between the microstructural unit in CGHAZ and the crack path using various steels, including bainitic steel. They clearly defined the crystallographic packet known as the Bain zone[2] as a microstructural unit and demonstrated the crack deviation/arrest capabilities of Bain-zone boundaries. This capability has also been verified by other researchers.[3–6] The deviation/arrest capabilities of a second phase such as carbide or martensite–austenite (M–A) constituents have also been reported,[7,8] and a crack initiation and propagation model based on the weakest-link assumption has been presented.[9,10] However, one of the

authors of the present study showed that the close-packed plane (CP) boundaries in one Bain zone was the formation site of a blocky-type M–A constituent in the case of a slow cooling rate, where granular bainite forms.[11,12] The existence of this formation site was attributed to the fact that the CP boundaries have a maximum misorientation of approximately 20 deg if Kurdjumov–Sachs orientation relationships (K–S ORs) are assumed.[13–15] Thus, CP boundaries in one Bain zone are also expected to strongly influence the crack path. However, the literature contains few studies on the effect of CP boundaries in a Bain zone on the crack path.

In the present study, for a prior austenite grain of a few hundred micrometers, we visualized and discussed the global effect of Bain-zone boundaries and the local effect of CP grain boundaries on the path of secondary cleavage cracks (observed on a fractured V-notch Charpy specimen). We subsequently discuss a correlation between CP boundaries and sites that favored formation of the blocky M–A constituents.

II. EXPERIMENTAL PROCEDURES

Bainitic steel with composition Fe-0.1C-0.3Si-0.25Cu-1.0Ni-0.4Cr-0.4Mo-0.039V (mass pct) was used. It was austenitized at 1623 K (1350 °C) for 30 second and then cooled at 1.67 K/s to room temperature, which simulated the CGHAZ of a weld with high heat input. The thermal cycle was applied using a radio-frequency heating apparatus. The Charpy V-notch impact test was conducted at 273 K (0 °C) using the sub-size $7.5 \times 10 \times 55$ mm specimen. EBSD measurements were performed in the vicinity of secondary cleavage cracks observed on the fractured V-notch Charpy specimen. The scanning electron microscope (SEM: JEOL JSM-7001F) equipped with a TSL EBSD system was used at an acceleration voltage of 15 kV and a step size of 100 nm. No cleanup was performed on the as-

HIDENORI TERASAKI, Associate Professor, YUTARO SHINTOME, Graduate Student, and YU-ICHI KOMIZO, Professor, are with the Joining and Welding Research Institute, Osaka University, 11-1 Mihogaoka, Osaka, Ibaraki 567-0047, Japan. Contact e-mail: hidenori@jwri.osaka-u.ac.jp MITSURU OHATA, Associate Professor, is with the Graduate School of Engineering, Osaka University, Osaka, Japan. KOJI MORIGUCHI, Chief Researcher, and YUSAKU TOMIO, Researcher, are with the Technical Research & Development Bureau, Nippon Steel & Sumitomo Metal Corporation, Tokyo, Japan.
Manuscript submitted August 29, 2014.
Article published online February 26, 2015.

acquired dataset. Points with a low confidence index (<0.1) were excluded to ensure the reliability of the phase determination. The K–S OR determines the 24 possible orientations of ferrite (variants) within a single austenite grain. In the present study, the variant number (V) in K–S OR follows the notation described by Morito et al.[13] The ferrite variants pair in one Bain zone according to this nomenclature is listed in Table I. The different colors indicate different CPs, as shown in the color key in Table I. Therefore, in one Bain zone, the maximum misorientation is 21.1 deg around the rotation axis of [0.91, −0.41, 0.00] in the K–S OR between V1 and V24.[13–15] In the present study, the boundaries

whose misorientations are shown in Table I are referred as "middle-angle" boundaries.

III. RESULTS AND DISCUSSION

Figure 1 shows optical microscope (OM) images of the microstructure containing secondary cleavage cracks. An SEM image of the fracture surface is also included in the top of the figure. The Charpy energy was 35 J at 273 K (0 °C). Granular bainite formed as a result of the slow cooling rate[12] and Figure 2 shows transmission electron microscope images of bainitic ferrite. The dashed white line in Figure 1 shows the prior austenite grain boundary (PAGB), and the large secondary cleavage crack is surrounded by this large PAGB. Therefore, we obtained a clear pole figure of the K–S OR from this target PAG, as shown in Figure 3; this pole figure was used for constructing a macrostructural unit map, such as Bain and CP map, along the method described by Takayama et al.[15]

Figure 4 shows an alpha-orientation map of the target PAG. The {001}-plane trace is indicated with a white line. As evident in the figure, the secondary cleave crack and the {001} trace are almost parallel. Figure 5 shows a cross-sectional view of the crack sectioned toward the arrow shown in Figure 4; the scanning ion microscopy (SIM) image was collected using the focused ion beam (FIB) method. The trace we observed on the surface clearly represents a whole crack path. The results in Figure 4 also reveal the global change and local change of the crack path. The global change is attributable to the Bain-zone boundaries, as pointed out by Gourgues et al.[1] The local changes always occur at misorientation boundaries, as shown in Figure 3. Therefore, the local changes in the crack path are expected to be due to the CP boundaries because the crack path contains the aforementioned "middle-angle" boundaries, which are

Table I. Ferrite Variants Pair in One Bain Zone

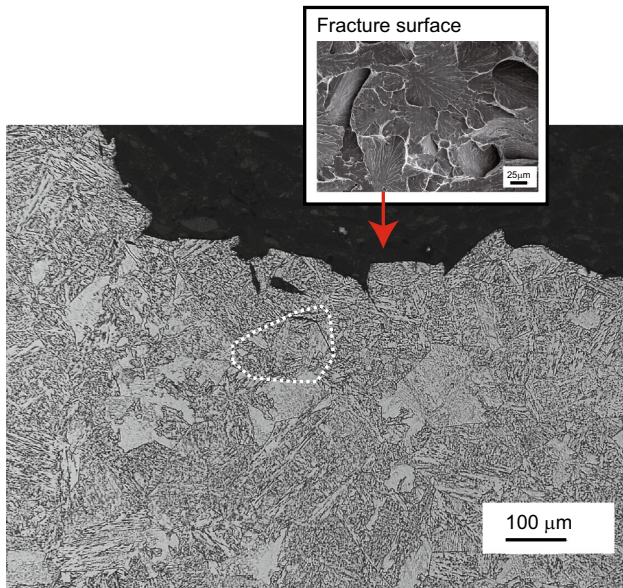| Variant pair in one Bain zone	[Rotation axis]/rotation angle in K-S OR [deg]
V1-V4	[0.000, -0.707, -0.707] / 10.5
V1-V8	[0.577, 0.577, -0.577] / 10.5
V1-V11	[0.933, 0.354, 0.065] / 14.9
V1-V13	[0.354, -0.933, -0.065] / 14.9
V1-V16	[0.659, -0.659, -0.363] / 20.6
V1-V21	[0.955, 0.000, -0.296] / 20.6
V1-V24	[0.912, -0.410, 0.000] / 21.1

.

Fracture surface

Fig. 1—OM side-view images of the microstructure of the fractured V-notch Charpy specimen. SEM image of the fracture surface is also included in the top of the figure. The dashed line encloses a target grain with a secondary cleavage crack.
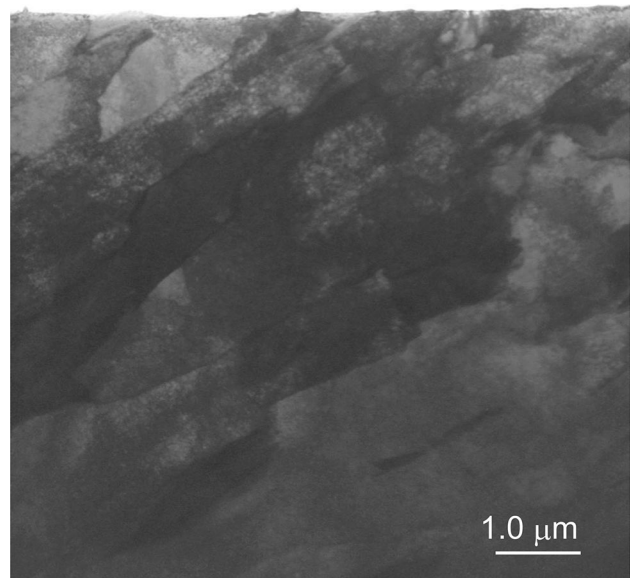

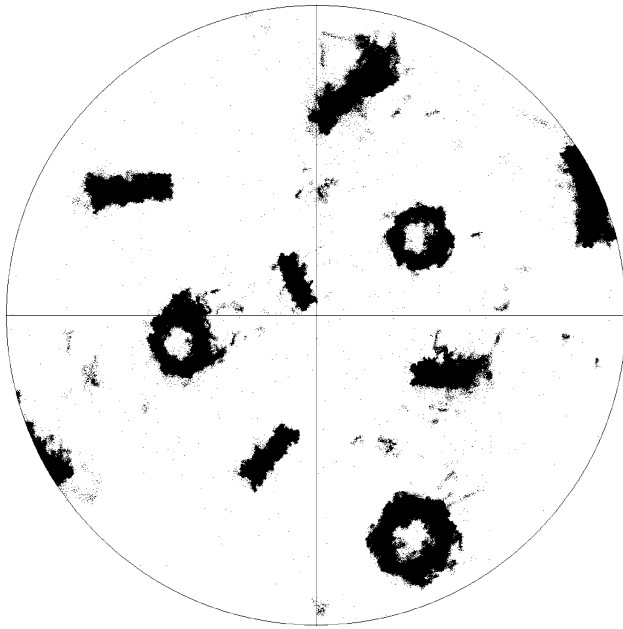Fig. 2—TEM images of bainitic ferrites.

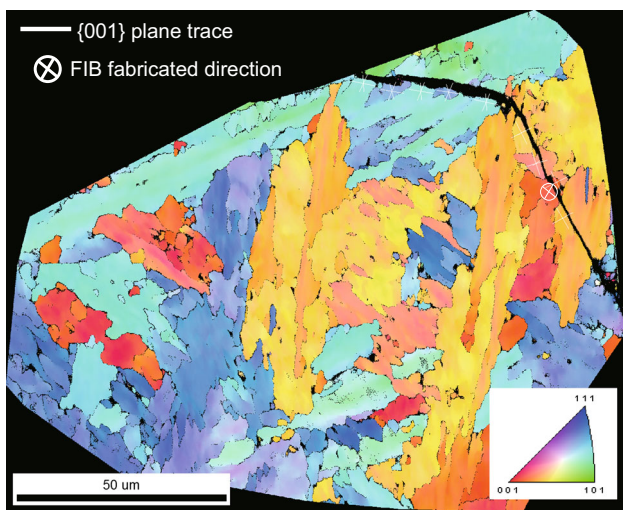Fig. 3—⟨001⟩ A Pole figure collected from target PAG shown in Fig. 1.

Fig. 5—Cross-sectional SIM image of a crack visualized using the FIB method. The arrow is compatible to the mark shown in Fig. 4.
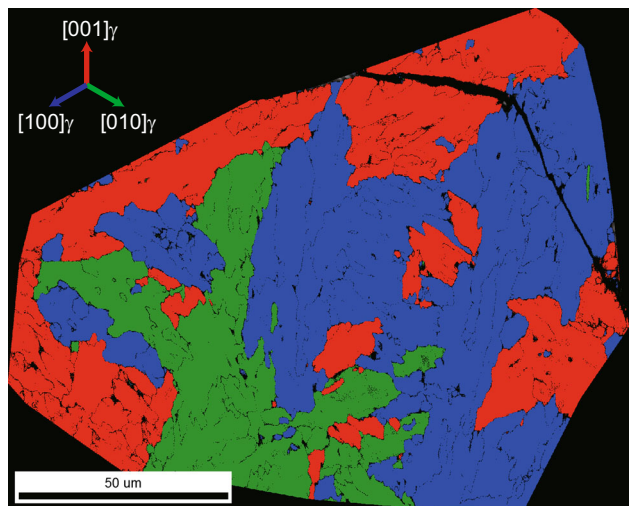

Fig. 4—Alpha-orientation map of the target grain; a trace of the {001} plane is also included.

Fig. 6—Bain-zone map of granular bainite.

formation site of blocky M–A constituents. We attempted to visualize these features by highlighting the bainitic ferrite lath of the same Bain zone in the Bain map and that of the same CP in the CP map.

The Bain map used to visualize the Bain zone is shown in Figure 6. As shown in the color key, K–S OR variants in the single PAG are classified by their corresponding lattice variants in reference to [001]gamma (red), [100]gamma (blue), and [010]gamma (green). As visualized in Figure 6, a global change in the crack path occurred at each Bain-zone boundary, as expected. The crack appears to propagate from left to right in Figure 6 because the width of the crack decreased from approximately 2.6 to 0.71 μm. Large energy dissipation

apparently occurred at the Bain-zone boundaries. However, determination of the crack propagation direction from only this result is difficult. In the present study, we only focus on the change in the crack path.

To visualize the source of the local changes in the crack path, we constructed a CP map,[15] as shown in Figure 7. Variants in the same CP are colored as indicated in the color key. CP 1, 2, 3, and 4 correspond to the (111), (1−11), (−111), and (11−1) planes, respectively. As expected, the CP boundaries always induce a local change in the crack path, as clearly shown in Figure 7. One factor that affects the local change is the "middle-angle" boundary. Another factor is the presence of M–A particles, as previously described.

Typical CP boundaries are indicated by white arrows in Figure 7, and each point indicated by an arrow was observed using SEM.

Figure 8 shows SEM images superimposed on the CP map shown in Figure 7. The arrow corresponds to that
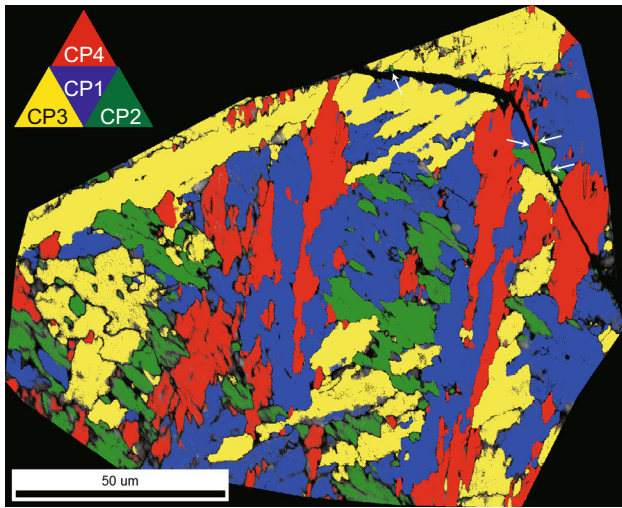

Fig. 7—CP map of granular bainite.

in Figure 7. As indicated by arrows in Figures 8(a) and (b), each CP boundary contained blocky M–A, as predicted. The correlation between the formation of blocky M–A constituents and characteristics of variant boundaries in one Bain-zone[11,12] was reconfirmed. Thus, these two factors are both attributed to the local change in the crack path. These observations also indicate that these two factors cannot be separated in the case of slow cooling conditions during the simulated CGHAZ in which granular bainite is formed. These two crack deviation/local changing factors are paired. The green dashed line in Figure 8(a) shows a small fraction of bainitic ferrite with a habit plane that differs from that of the surrounding bainitic ferrite. This fraction is also identified in the CP map in Figure 7. It is a typical formation site of blocky M–A. As shown in Figure 8(a), four blocky M–A regions surround the green dashed line and cause crack deviation.

The crack deflection occurred in the center of Figure 8(c) was attributed to the global change of crack path at the Bain boundary. On the other hand, the blue dashed line in Figure 8(c) shows the V1 to V4 boundary. As shown in Table I, its misorientation angle is equivalent to that of the CP boundary of V1 to V8. Therefore, the V1 to V4 boundary also favors formation of the blocky M–A constituent and we can confirm the
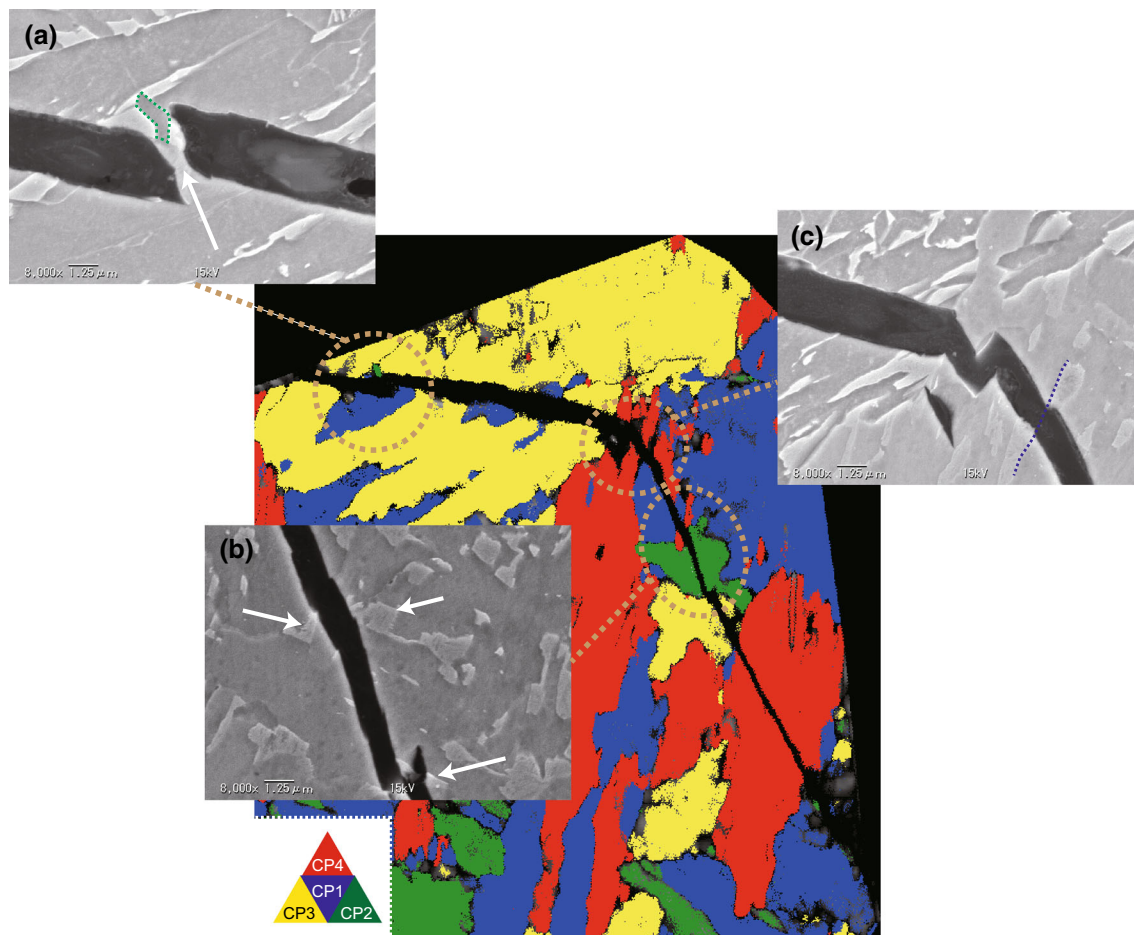

Fig. 8—(a, b) SEM image of the blocky M–A constituent at the CP boundaries. (c) V1 to V4 boundaries (blue dashed line).
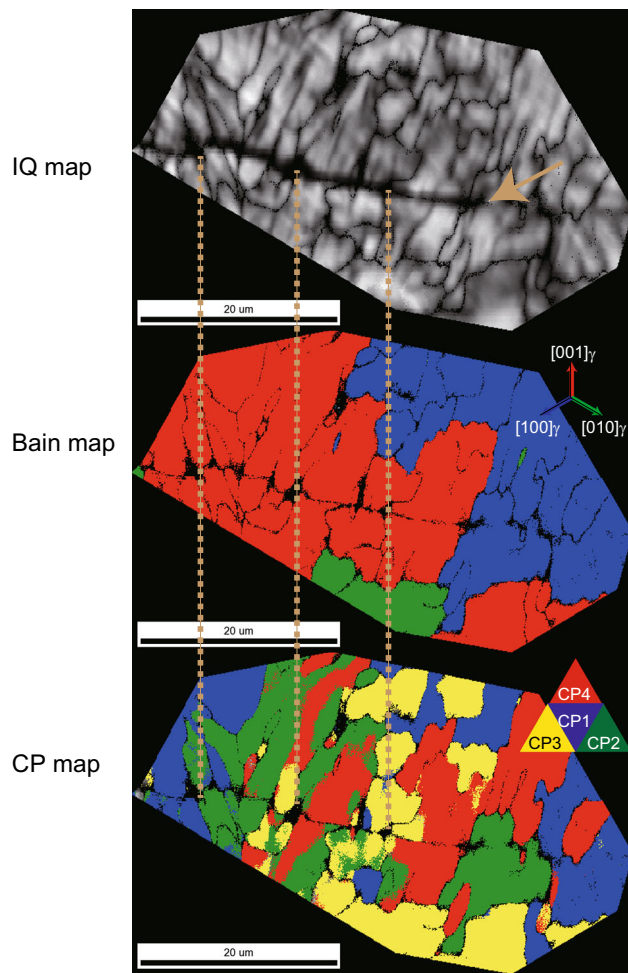
Fig. 9—Other example of local change in crack path shown by image quality (IQ), Bain, and CP maps.

with a larger Bain-zone area, as demonstrated in the present study. These results highlight a controversial problem that we will address further in our future work.

IV. CONCLUSIONS

A secondary cleavage crack with dimension of a few hundred micrometers was observed on a fractured V-notch Charpy specimen. Global and local changes in the crack path were analyzed and visualized using Bain-zone maps and CP maps. The source of the global change in the crack path was Bain-zone boundaries. However, the source of local changes in the crack path was CP boundaries and blocky M–A constituents in one Bain zone. Furthermore, a correlation between "middle-angle" boundaries and sites that favored formation of the blocky M–A constituents was confirmed. The obtained results indicate that these two crack deviation/local changing factors are paired in the case of slow cooling conditions for a simulated CGHAZ in which granular bainite is formed.

formation and local change of the crack path, as shown in Figure 8(c).

The blocky M–A constituent serves not only as an energy dissipation site for cracks but also as an initiation site.[7,16] Therefore, in this investigation, a determination of which role the observed M–A plays is difficult. However, we clarified that, when "middle-angle" boundaries are present, the formation of blocky M–A constituent and local changes in the crack path can be observed in one Bain zone.

Figure 9 shows other example of local change in the crack path (in different prior austenite grain from that in Figure 7), showing compatibility between image quality (IQ), Bain, and CP map. As indicated by three dashed lines in Figure 9, local change in the crack path occurred in one Bain zone and at CP boundary. The crack was arrested as indicated by an arrow in IQ map and it corresponded to the Bain boundary.

Reducing the Bain-zone area is important to enhance the toughness of the CGHAZ. However, high heat input welding results in slow cooling and in a microstructure

REFERENCES

1. A.F. Gourgues, H.M. Flower, and T.C. Lindley: *Mater. Sci. Technol.*, 2000, vol. 16, pp. 26–40.
2. A.F. Gourgues: *Mater. Sci. Technol.*, 2002, vol. 18, pp. 119–33.
3. A. Lambert, X. Garat, T. Sturel, A.F. Gourgues, and A. Gingell: *Scripta Mater.*, 2000, vol. 43, pp. 161–66.
4. J. Nohava, P. Hausild, M. Karlik, and P. Bompard: *Mater. Charact.*, 2002, vol. 49, pp. 211–17.
5. A. Lambert-Perlade, A.F. Gourgues, and A. Pineau: *Acta Mater.*, 2004, vol. 52, pp. 2337–48.
6. L. Rancel, M. Gomez, S.F. Medina, and I. Gutierrez: *Mater. Sci. Eng. A*, 2011, vol. 530, pp. 21–27.
7. C.L. Davis and J.E. King: *Metall. Mater. Trans. A*, 1994, vol. 25A, pp. 563–73.
8. Y. Li and T.N. Baker: *Mater. Sci. Technol.*, 2010, vol. 26, pp. 1029–40.
9. A. Lambert-Perlade, A.F. Gourgues, J. Besson, T. Sturel, and A. Pineau: *Metall. Mater. Trans. A*, 2004, vol. 35A, pp. 1039–53.
10. A. Pineau: *Int. J. Fract.*, 2006, vol. 138, pp. 139–66.
11. H. Terasaki and Y. Komizo: *Metall. Mater. Trans. A*, 2013, vol. 44A, pp. 5289–93.
12. H. Terasaki and Y. Komizo: *Metall. Mater. Trans. A*, 2013, vol. 44A, pp. 2683–89.
13. S. Morito, H. Tanaka, R. Konishi, T. Furuhara, and T. Maki: *Acta Mater.*, 2003, vol. 51, pp. 1789–99.
14. A. Stormvinter, G. Miyamoto, T. Furuhara, P. Hedstrom, and A. Borgenstam: *Acta Mater.*, 2012, vol. 60, pp. 7265–74.
15. N. Takayama, G. Miyamoto, and T. Furuhara: *Acta Mater.*, 2012, vol. 60, pp. 2387–96.
16. L.Y. Lan, C.L. Qiu, D.W. Zhao, X.H. Gao, and L.X. Du: *J. Mater. Sci.*, 2012, vol. 47, pp. 4732–42.